AIMS Materials Science

AIMS Materials Science, 10(1): 55–69.
DOI: 10.3934/matersci.2023004
Received: 06 July 2022
Revised: 30 November 2022
Accepted: 16 December 2022
Published: 29 December 2022

http://www.aimspress.com/journal/Materials

Research article

Effect of sub-zero treatments on hardness and corrosion properties of low-alloy nickel steel

Vinda Puspasari[1,*], Satrio Herbirowo[1], Alvin Muhammad Habieb[1,2], Dedi Pria Utama[1], Rahadian Roberto[1] and Bintang Adjiantoro[1]

[1] Research Center for Metallurgy and Materials, National Research and Innovation Agency, Gedung 470, South Tangerang, Banten, 15314, Indonesia
[2] Nano Center Indonesia, South Tangerang, Banten, 15314, Indonesia

* **Correspondence:** Email: vind001@brin.go.id; Tel: +62 896-2532-4187.

Abstract: Low alloy nickel steel was chosen for this experiment because it is suitable for grinding balls application due to its high hardness and corrosion resistance. This study aimed to see the effect of different sub-zero treatments on the hardness, fractography and corrosion properties of low alloy nickel steel. The prepared specimens were heated to the austenitizing temperature of 980 ℃ in a furnace for one hour and water-quenched until they reached room temperature. Furthermore, the quenched specimens were chilled in liquid nitrogen for a variated time of 10, 60 or 360 min, followed by tempering treatment at 200 ℃ for one hour. According to the hardness test, the sub-zero treatment is effective in hardening materials, where the hardness value increases as the sub-zero treatment time increases, ranging from 204.93 to 417.98 HV. The fractography test indicated ductile fracture characterized by dimples at the fractured surface. Moreover, the corrosion test showed an enhancement of corrosion resistance with increased sub-zero treatment time.

Keywords: sub-zero treatment; grinding ball; hardness; fractography; corrosion

1. Introduction

Grinding in the milling process is an essential process to reduce the sizes of particles in mining metallurgy, the cement industry and the chemical and power industries using steel grinding balls [1]. Almost half of the world's milling circuits use ball mills, and 90% of mining operations utilize balls as grinding devices [2]. One of the most popular milling machines is the cement mill, which is used to crush raw materials such as lime, silicate, alumina and iron oxide using grinding balls [3]. The quality and efficiency of the grinding process are greatly affected by the grade and characteristics of grinding balls [4]. The minerals usually have high hardness, meaning the grinding ball must maintain its shape during the milling process [5]. Therefore, the grinding balls must meet the requirements such as good hardness and corrosion resistance [6].

Grinding balls are commonly made from low alloy steel with different carbon contents (0.7 to 0.8 wt%) and alloyed with manganese, chromium (up to 1 wt%), molybdenum (up to 0.025 wt%) and copper (up to 1 wt%) [7]. The alloying method is useful not only to maintain a suitable value of hardness but also to improve corrosion resistance along the ball cross-section [8]. The low alloy nickel steel was chosen in this experiment because it performs better than high carbon martensitic iron for grinding ball application due to the work hardening effect during the service [9]. Furthermore, the presence of chromium and nickel in these alloys will significantly improve mechanical properties and corrosion resistance [10]. According to the previous work, the low alloy steels are proven to have high hardness and abrasion resistance properties, which are suitable for grinding balls [11]. The addition of Cr, Mo and Cu also affects the hardness gradient of the grinding ball from the hard surface (martensite) to the soft core (perlite) [12].

The critical factor in grinding ball application is the total wear of the grinding balls, which consists of abrasion, corrosion and impact properties [13]. For that reason, it is hard to divide the contributions of each mechanism toward wear properties [14]. The corrosion and dissolution of metal surfaces during grinding becomes more than half of the complete wear of grinding balls [15]. The corrosion mechanism is also important to explore because of its significant effect on the total wear of grinding balls [16]. Furthermore, to obtain the best performance and durability of grinding balls, the affecting factors such as fabricating methods based on properties, heat treatment and chemical composition become crucial [5]. In this paper, the value of hardness, surface cracking and corrosion properties will be evaluated.

The utilization of heat treatment with the rolled steel balls, such as quenching followed by tempering, is appropriate to enhance the mechanical properties [17]. The addition of sub-zero treatment as the hardening treatment to the grinding balls is believed to enhance the durability of grinding balls [18]. Sub-zero treatment (also called cryogenic treatment) refers to the treatment process at low temperatures (lower than −80 ℃) added to the conventional heat treatment (CHT) [19]. The effect of the sub-zero treatment can cause a significant reduction of the retained austenite and martensite refinement and balance out the products [20]. The essential factor in sub-zero treatment is that the treatment should be done as quickly as possible after quenching to avoid the degradation of the properties of materials [21]. This study investigated the effects of different sub-zero treatments on the hardness, fractography and corrosion properties of low alloy nickel steel.

2. Materials and methods

The chemical composition of low alloy nickel steel is presented in Table 1. The process was started by specimen preparation using the machining process to customize sample testing standards. The prepared specimens were subjected to the conventional heat treatment, which consisted of gradual heating up to the austenitizing temperature of 980 ℃ in the furnace for 1 h. Then, the specimens were quenched until they reached room temperature using water. After that, the quenched specimens were cooled using liquid nitrogen for 10 (C10), 60 (C60) and 360 (C360) min. Furthermore, the Fe-Ni-Cr-Mo specimens were removed from the nitrogen reaction tube and placed in the open air until their temperature reached room temperature. Then, the Fe-Ni-Cr-Mo specimens were tempered at 200 ℃ for 1 h to minimize residual stress.

Table 1. Chemical compositions of Fe-Ni-Cr-Mo specimens.

Specimen	Al (wt%)	Mn (wt%)	Si (wt%)	Cr (wt%)	Ni (wt%)	Mo (wt%)	C (wt%)	Fe (wt%)
FeNiCrMo-3	0.01	0.35	0.42	0.03	2.26	0.0008	0.02	Bal.
FeNiCrMo-4	0.08	0.47	0.48	1.23	2.03	0.89	0.04	Bal.

The mechanical properties of samples were examined using the micro-Vickers test with 0.3 kN of loading and 10 s of pressing time. The fractography images of specimens after the impact test were observed using SEM-EDS. Furthermore, the electrochemical measurement test was done using the Gamry G750 corrosion measurement system in 3.5% NaCl solution. The 1.1 cm^2 specimens were cut using a cutting machine and installed to copper wire for electrical contact. After that, the specimens were mounted using resin to cover the unexposed area. The mounted specimens were ground using 120–1200 grit SiC paper with the help of distilled water. Electrochemical measurements were performed using GAMRY Series G-750 Corrosion Measurement System. The electrochemical measurement utilized Pt electrode as the counter electrode, saturated calomel as the reference electrode and the specimens as the working electrode. The open-circuit potential (Eocp) was measured, which is continued by the Tafel polarization and cyclic polarization test. The potentiodynamic polarization test was performed at a scan rate of 1 mV/s in ±250 mV from the OCP potential. The measurement of cyclic polarization was done based on ASTM G-61 using potential of −500 mV to +1500 mV, current density of 10 mA/cm^2, forward scan rate of 5 mV/s and reverse scan of 2.5 mV/s. The corroded samples were observed using SEM-EDS to determine corrosion morphology and elements contained in corrosion products.

3. Results and discussion

3.1. Effect of sub-zero treatment on micro-Vickers hardness test results

The hardness properties were characterized using micro-Vickers at six spot locations, and the averaged value was calculated. The labels of specimens showed the time of sub-zero treatment and material type; for instance, C10-3 indicated 10 min of sub-zero treatment and FeNiCrMo-3 specimens. The analytical graph of micro-Vickers results was also processed using IBM-SPSS statistical software and the normality test method using Kolmogorov-Smirnov and Shapiro-Wilk.

Figure 1 illustrates the results of the micro-Vickers hardness test of FeNiCrMo specimens that experienced the sub-zero treatment process, as illustrated. The sub-zero treatment is effective in hardening materials, where the hardness value increases as the sub-zero treatment time increases. The hardness value of FeNiCrMo-3 specimens shows values of 204.93 for C10, 228.18 for C60, and 238.55 for C360, indicating an increase in hardness value. An increase of hardness with increasing sub-zero treatment time can enhance plastic deformation resistance because of restricted dislocation movement [22]. The longer the sub-zero treatment duration is, the more dislocation movement is prevented, resulting in a greater hardness value. The hardness and modulus values dropped as the indenter displacement expanded [23]. Furthermore, the enhancement of flow stress (α hardness) with decreasing temperatures can also enhance sub-zero treatment specimen's wear and friction behavior [24].

The hardness values of FeNiCrMo-4 specimens show the values of 390.27 for C10, 417.98 for C60 and 333.65 for C360. The hardness value of FeNiCrMo-4 specimens with 60 minutes of sub-zero treatment time is the highest of all the specimens worth 418 Hv. The increase of hardness value is caused by the uniform distribution and refinement of the grains after sub-zero treatment [25]. The hardness value of FeNiCrMo-4 specimens is higher than FeNiCrMo-3 with the same sub-zero treatment time. This phenomenon is affected by CrMo chemical composition in the alloy, where the FeNiCrMo-4 specimens have a higher content of element alloying [26]. Table 2 shows that the significance value is above 0.05 using Kolmogorov-Smirnov and Shapiro-Wilk normality test, so the hardness properties results are normally distributed. Table 3 shows the results of ANOVA for hardness using micro-Vickers hardness measurements, which reveals that the Sig value <α (0.05) proves the variation in process treatment has an effect.

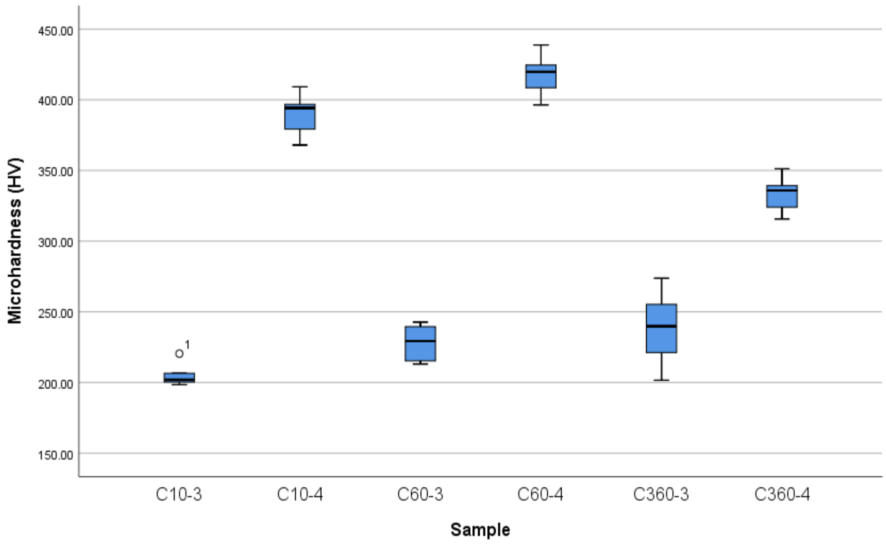

Figure 1. The hardness properties of the FeNiCrMo with various quenched.

Table 2. The hardness test data of FeNiCrMo with normality test.

	Specimens	Kolmogorov-Smirnov[a]			Shapiro-Wilk		
		Statistic	df	Sig.	Statistic	df	Sig.
Hardness	C10-3	0.261	6	0.200*	0.789	6	0.047
	C10-4	0.222	6	0.200*	0.953	6	0.765
	C60-3	0.276	6	0.169	0.837	6	0.123
	C60-4	0.159	6	0.200*	0.986	6	0.978
	C360-3	0.158	6	0.200*	0.987	6	0.980
	C360-4	0.200	6	0.200*	0.973	6	0.910

*This is a lower bound of the true significance.

Table 3. The hardness test data of FeNiCrMo with one-way ANOVA test.

Hardness	Sum of squares	df	Mean square	F	Sig.
Between groups	246847.152	5	49369.430	197.946	0.000019
Within groups	7482.253	30	249.408		
Total	254329.406	35			

3.2. Effect of Sub-zero treatment on fractography of Fe-Ni-Cr-Mo results

Figure 2a–d indicates SEM characterization results of low alloy nickel steel specimens' fracture surfaces, showing dimples (black arrows) and brittle fracture (red arrows) in all specimens. Figure 2a characterizes ductile fracture, which reveals dimples (black arrows) in the fractured surface for the FeNiCrMo C10-4 sample. Figure 2c shows fine dimples (black arrows) in the fractured surface conforming to ductile fracture characteristics. This phenomenon is caused by increased formability from low alloy nickel steel alloy and the temperature sensitivity of stress required for dislocation motion [27]. The shorter time of sub-zero treatment causes lower stress involved to move dislocation, which causes deformation is preferred. Figure 2b,d indicate ductile tearing and quasi-cleavage facets [28]. This phenomenon happened due to the enhancement of sub-zero treatment time, which increases the difficulty in cross slip in the material, affecting the enhancement of flow stress, strain hardening exponent, and decreasing the plasticity of materials [29].

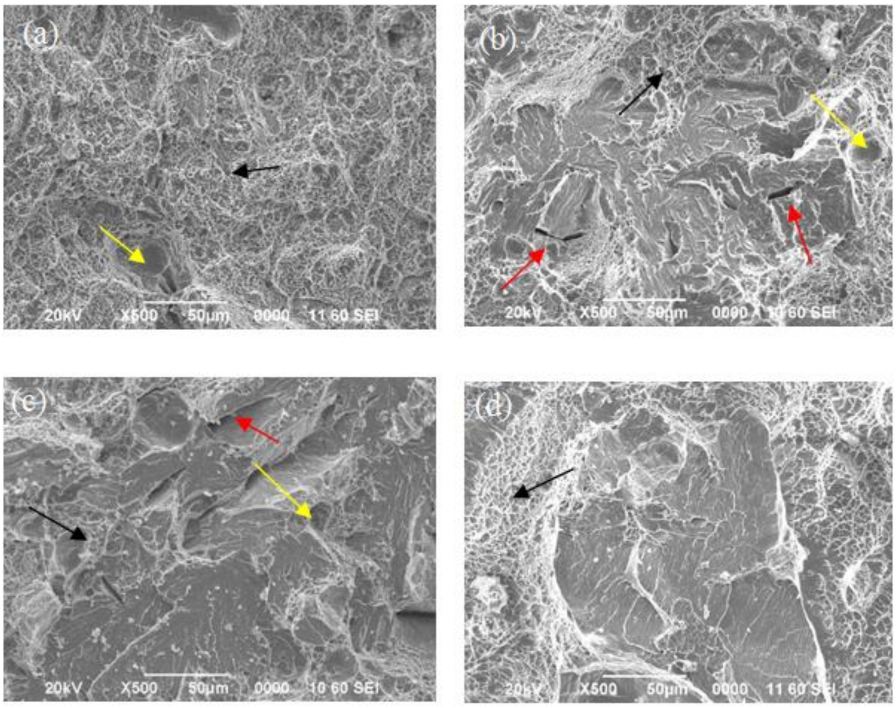

Figure 2. Fractography images of (a) FeNiCrMo C10-3, (b) FeNiCrMo C60-3, (c) FeNiCrMo C10-4, (d) FeNiCrMo C60-4 showing topological changes.

The microvoids with spherical shapes were also found in Figure 2a–c with yellow arrow marks, but Figure 2d is not showing the microvoids. The microvoids were formed in heterogeneous areas where the size and distribution of heterogeneities influence void formation, growth and coalescence [30]. The higher hardness of the matrix will enhance the number of voids required to propagate a fracture [22]. Figure 3a–d refers to EDS mapping of low alloy nickel steel fracture surfaces. Figure 3a,b indicates C, Fe and Ni elements in the specimens where the dark areas are less elemental. Figure 3c,d shows the elements C, Cr, Fe, Ni and Mn evenly distributed in the FeNiCrMo-4 specimens.

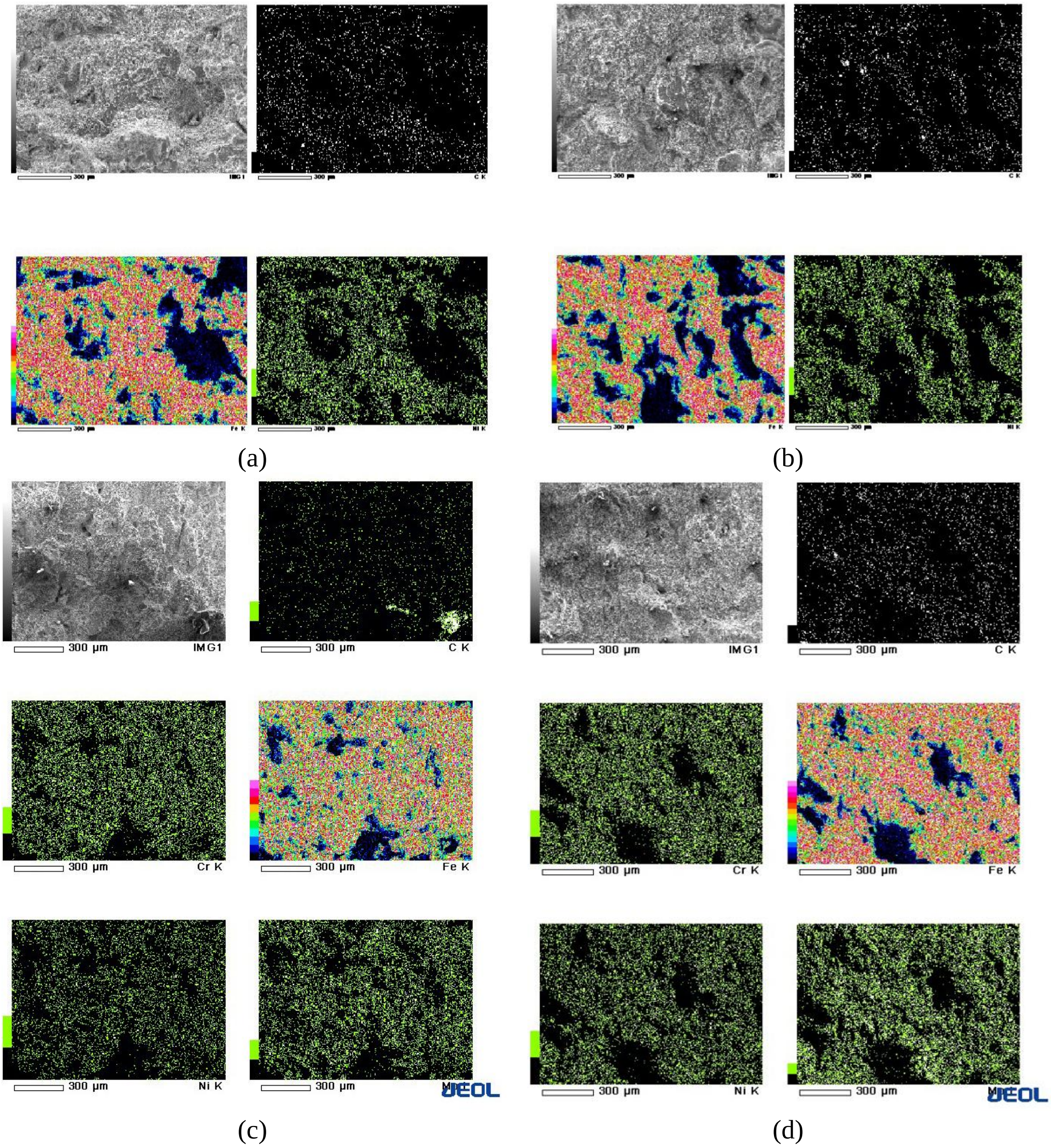

Figure 3. EDS Mapping of crack surfaces of (a) FeNiCrMo C10-3, (b) FeNiCrMo C60-3, (c) FeNiCrMo C10-4 and (d) FeNiCrMo C60-4.

3.3. Effect of Sub-zero treatment on microstructure experimental results

Figure 4a–f reveals the morphological structure of FeNiCrMo alloy with different times of cryogenic treatment using liquid nitrogen as the cooling medium, showing the existence of martensite (red arrows), ferrite (yellow arrows) and retained austenite (blue arrows). The cryogenic heat treatments contributed to the phase transformation, where the retained austenite was transformed into lath martensite. There was an increase in martensite amount with the rise in cryogenic time (10–360 min), which is caused by how long the austenitization process had taken [31]. The lath martensite was also transformed into the lath martensite tempered due to the tempering process after cryogenic treatment [32].

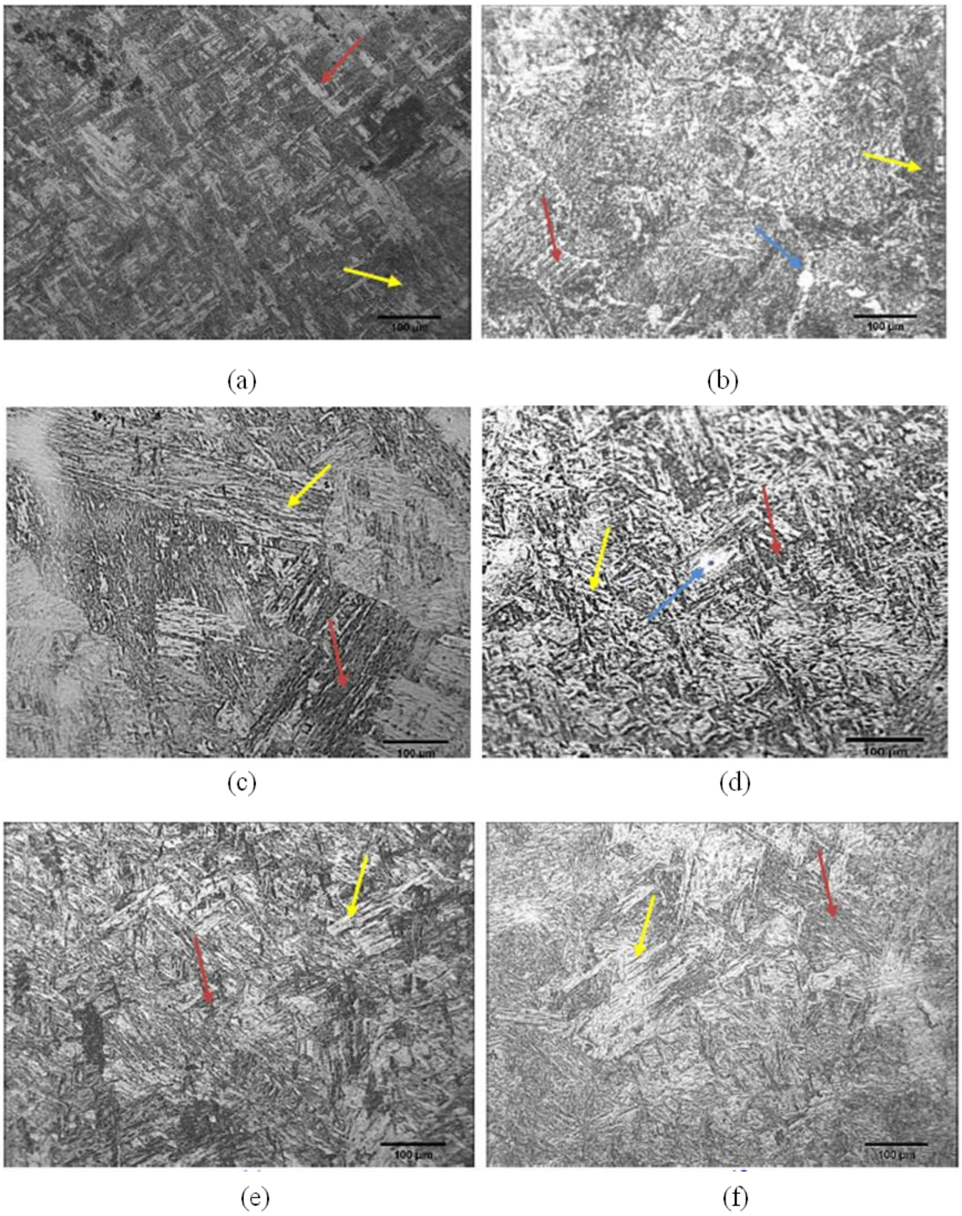

Figure 4. Microstructure of (a) FeNiCrMo C10-3, (b) FeNiCrMo C60-3, (c) FeNiCrMo C10-4, (d) FeNiCrMo C60-4, (f) FeNiCrMo C-360-3, (g) FeNiCrMo C-360-4.

Furthermore, it also can be seen that there was a gradual decrease in retained austenite in the FeNiCrMo specimens with the enhancement in soaking time [33]. The deep cryogenic treatment using nitrogen showed that the martensite formed soon after the cooling process and having the body-centered tetragonal crystal structure. After the tempering process was done, the body-centered tetragonal martensite was transformed into body-centered cubic martensite, which also affects its hardness [34].

3.4. Effect of Sub-zero treatment on corrosion test results

Open circuit potential (OCP) was an important factor in comprehending the material's tendency to corrode [35]. The more positive the value of open circuit potential is, the more difficult the material is to corrode [36]. Based on the Pourbaix diagram of the Fe-Cl system, the range potential for OCP in this study is in the formation of Fe^{2+} [37].

Figure 5a indicates the curve of open circuit potential of Fe-Ni-Cr-Mo specimens in 3.5% NaCl solution. The Eocp values of FeNiCrMo-3 specimens are −585 mV for C10-3, −554 mV for C60-3 and −547 mV for C360-3. Furthermore, the Eocp values of FeNiCrMo-4 specimens are −599 mV for C10-4, −567 mV for C60-4 and −505 mV for C360-4. The Eocp value increases with the increasing of sub-zero treatment time. This phenomenon proves that the higher time of sub-zero treatment causes the specimens nobler than the lower time of sub-zero treatment [38]. The FeNiCrMo-4 specimens have a higher value of Eocp, for the same time of sub-zero treatment, than FeNiCrMo-3. This phenomenon is caused by higher Cr and Mo content in FeNiCrMo-4 specimens, which affects the specimens' corrosion resistance. These results reveal that FeNiCrMo-4 specimens were less reactive than FeNiCrMo-3.

In this work, the electrochemical corrosion parameters such as corrosion potential (Ecorr) and corrosion current densities (Icorr) were automatically obtained from Butler-Volmer and Tafel equations [39]. The next step of Tafel slope analysis and fitting of the polarization curves were analyzed using Echem analyst software to acquire the corrosion rate of Low alloy nickel steel. Figure 5b shows that the FeNiCrMo-4 specimens with 360 min of sub-zero treatment time manifest higher corrosion potential than FeNiCrMo-4 specimens with 10- and 60-minute sub-zero treatment time, as well as FeNiCrMo-3 specimens. It is also shown in Table 4 that the corrosion current decreases with the increase of sub-zero treatment time, suggesting that the sub-zero treatment time variation improves the corrosion behavior of the specimens [40]. The corrosion rate decreases as the sub-zero treatment time increases, indicating better corrosion resistance. The highest corrosion resistance is FeNiCrMo C360-4, worth 1.759 mpy, caused by the highest protective passive film due to its high content of Cr [16].

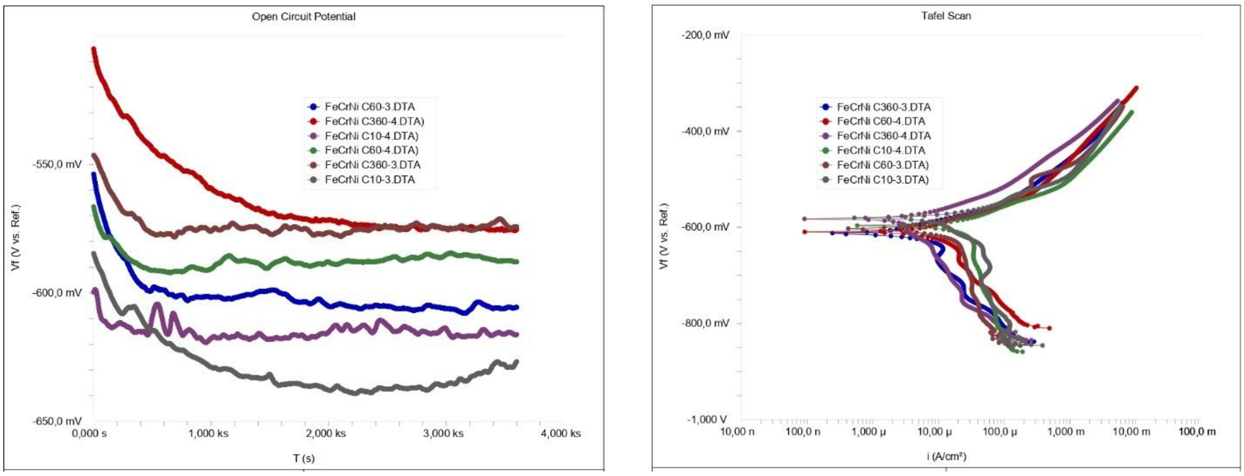

(a) (b)

Figure 5. (a) Open circuit potential measurement, (b) Tafel polarization curve of low alloy nickel steel specimens in 3.5% NaCl solution.

Table 4. Electrochemical parameters obtained from Tafel polarization test of Fe-Ni-Cr-Mo specimens in 3.5% NaCl solution.

Specimens	Ecorr (mV)	Icorr (μA/cm^2)	Corr rate (mpy)
FeNiCrMo C10-3	−580.2	40.02	18.67
FeNiCrMo C10-4	−596.2	24.43	11.40
FeNiCrMo C60-3	−602.4	18.65	8.70
FeNiCrMo C60-4	−609.6	9.443	4.405
FeNiCrMo C360-3	−612.0	5.498	2.565
FeNiCrMo C360-4	−582.3	3.770	1.759

Figures 6a and 5b provide the cyclic polarization curves of low alloy nickel steel specimens in a 3.5% NaCl solution. All the FeNiCrMo-4 specimens in Figure 6b presented a substantial hysteresis loop between the forward and the reversed scans, which characterizes the material as generally susceptible to pitting corrosion [41]. Meanwhile, all the FeNiCrMo-3 specimens did not show a substantial hysteresis loop between the forward and reverse scans, which indicates no pitting corrosion is suspected. The Ecorr values of FeNiCrMo-3 specimens are −820.9 mV for C10-3, −820.1 mV for C60-3 and −734.5 mV for C360-3. Furthermore, the Ecorr values of FeNiCrMo-4 specimens are −834.5 mV for C10-4, −822.1 mV for C60-4 and −818.4 mV for C360-4.

As can be seen, the low alloy nickel steel with higher sub-zero treatment time has higher corrosion potential than low alloy nickel steel with lower sub-zero treatment time. This means that the corrosion resistance was improved with increasing sub-zero treatment time due to the microstructure of martensite and being free from retained austenite [42]. According to our previous work, the higher sub-zero treatment time eliminated retained austenite and achieved 98.617% of the martensite phase at 360 min of sub-zero treatment time [43]. Moreover, the value of repassivation potential in FeNiCrMo-4 specimens was shifted towards more noble potentials with the increasing sub-zero treatment time, which indicates the better resistance of the material to pit growth [12].

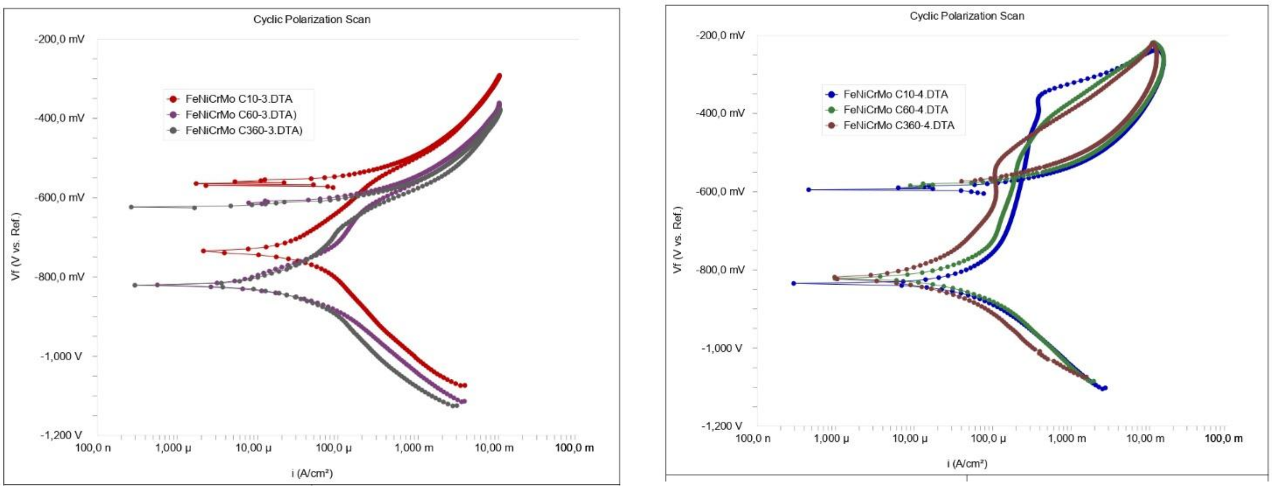

(a) (b)

Figure 6. Cyclic polarization curves of (a) FeNiCrMo-3 specimens and (b) FeNiCrMo-4 specimens in 3.5% NaCl solution.

3.5. Effect of Sub-zero treatment on SEM-EDS of corrosion products in Fe-Ni-Cr-Mo specimens

Figure 7a–f shows all the surfaces were covered by ion complexes, indicating that all surface regions have similar corrosion behavior and experienced uniform corrosion. The corroded area decreases with the increase of sub-zero treatment time. The surface of FeNiCrMo-4 specimens exhibited some small individual pits where it seemed that the size increased and the number of pits decreased after the longer sub-zero treatment time [22]. This phenomenon is caused by the distribution element and the effect of cold temperature quenching immersion affecting the phase transformation and carbon in the specimens, increasing the pitting corrosion size.

The EDS spectra reveal the presence of oxygen, which proves the corrosion product in all low alloy nickel steel specimens. The FeNiCrMo C10-3 sample showed the highest percentage (15.9%) of oxygen. The oxidized displays the most exceptional tribological performance because to the synergistic chemical change and mechanical strengthening by O atoms [44]. While the lowest 8.77% of oxygen was revealed by the FeNiCrMo C360-3. It is also displayed that the surface of the uniform corrosion contains natrium and chloride, which relate to the surface exposure in the 3.5% NaCl corrosive medium. The matrix is fully covered by corrosion products, while the corrosion products layer is not uniform [12].

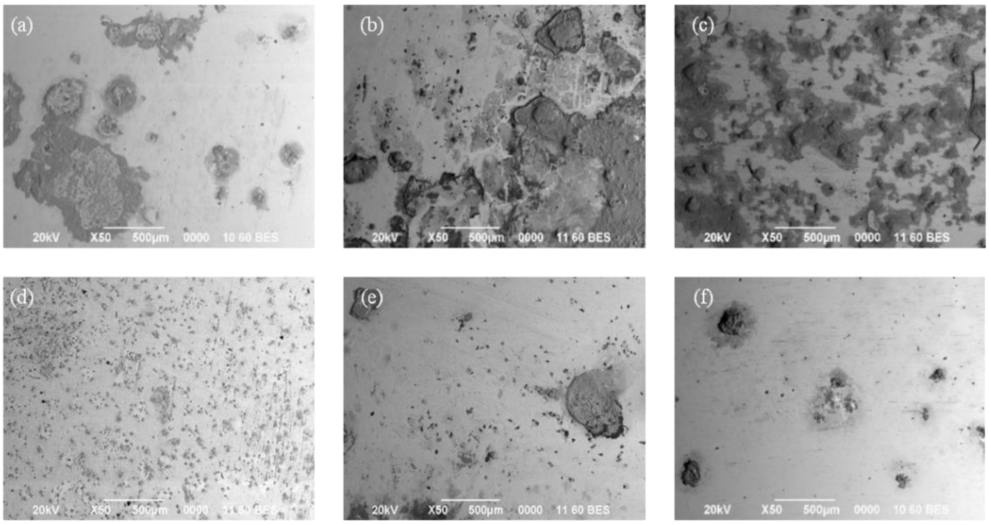

Figure 7. SEM images of (a) FeNiCrMo C10-3, (b) FeNiCrMo C60-3, (c) FeNiCrMo C360-3, (d) FeNiCrMo C10-4, (e) FeNiCrMo C60-4 and (f) FeNiCrMo C360-4 after immersing in 3.5% NaCl solution.

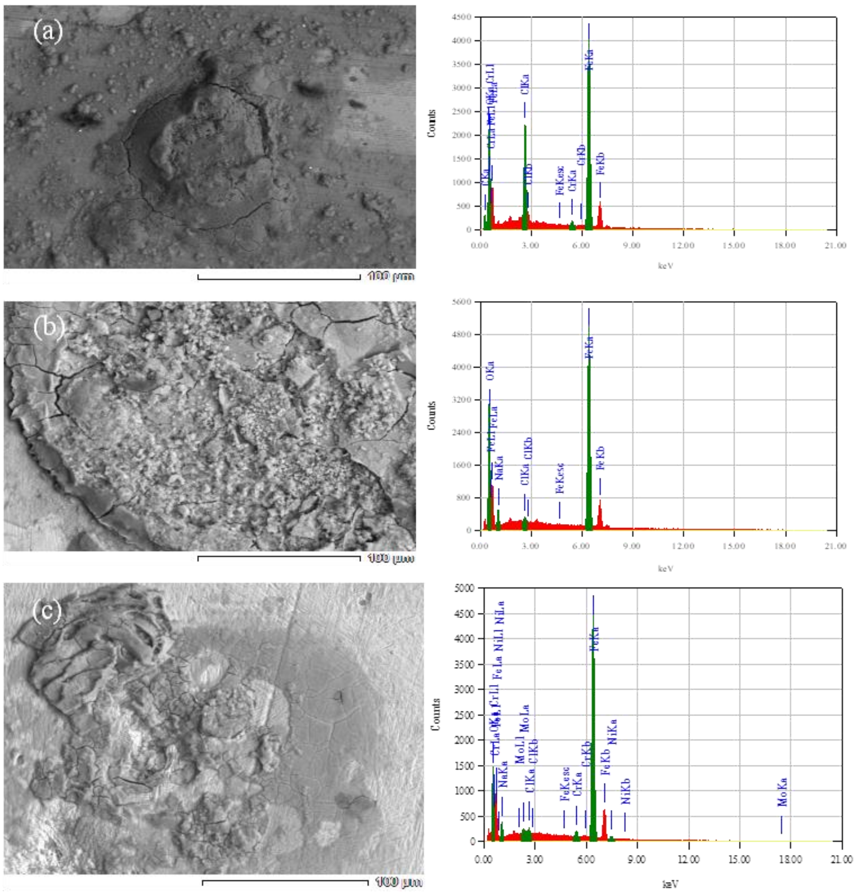

Element	Weight
O	15.9
Na	4.08
Cl	0.45
Fe	79.57

Element	Weight
O	15.82
C	9.81
Cl	8.28
Cr	0.95
Fe	65.14

Element	Weight
O	8.77
Na	3.49
Cl	0.42
Cr	1.21
Fe	82.91

Figure 8. EDS results of FeNiCrMo (a) C10-3, (b) C60-3 and (c) C360-3 after immerse in 3.5% NaCl solution.

4. Conclusions

This study investigated the effects of sub-zero treatment on the hardness, fractography morphology and corrosion properties of low alloy nickel steel. The results confirm that the hardness characterization data using the Kolmogorov-Smirnov and Shapiro-Wilk normality tests were normally distributed, with a Sig value of (0.05), indicating that the FeNiCrMo-4 with 60 min of immersion time is the highest of all the specimens worth of 417.9 HV. The corrosion rate of low alloy nickel steel with a longer sub-zero treatment time is lower than low alloy nickel steel with a shorter sub-zero treatment period. This phenomenon suggests that increasing the sub-zero treatment period improves corrosion resistance. As the sub-zero treatment period increased, the corroded area decreased.

Acknowledgments

The authors would like to express their gratitude to the National Research and Innovation Agency of Indonesia for their financial support. The main contributors in this paper are Vinda Puspasari and Satrio Herbirowo.

Conflicts of interests

All authors declare no conflicts of interest in this paper.

References

1. Kartikasari R, Subardi A, Wijaya AE (2021) Development of Fe-5Al-1C alloys for grinding ball. *Eastern-European J Enterp Technol* 1: 29–35. https://doi.org/10.15587/1729-4061.2021.225421
2. Foszcz D, Krawczykowski D, Gawenda T, et al. (2018) Analysis of process of grinding efficiency in ball and rod mills with various feed parameters. *IOP Conf Ser-Mater Sci Eng* 427: 012031. https://doi.org/10.1088/1757-899X/427/1/012031
3. Jankovic A, Wills T, Dikmen S (2016) A comparison of wear rates of ball mill grinding media. *J Min Metall A Min* 52: 1–10. https://doi.org/10.5937/JMMA1601001J
4. Zurnadzhy VI, Efremenko VG, Wu KM, et al. (2020) Quenching and partitioning-based heat treatment for rolled grinding steel balls. Metall Mater Trans A 51: 3042–3053. https://doi.org/10.1007/s11661-020-05737-w
5. Massola CP, Chaves AP, Albertin E (2016) A discussion on the measurement of grinding media wear. *J Mater Res Technol* 5: 282–288. https://doi.org/10.1016/j.jmrt.2015.12.003
6. Stalinskii DV, Rudyuk AS, Solenyi VK, et al. (2017) Improving the quality of steel grinding balls. *Steel Transl* 47: 130–136. https://doi.org/10.3103/S0967091217020115
7. Aissat S, Sadeddine A, Bradai MA, et al. (2017) Effect of heat treatment on the hardness and wear of grinding balls. *Met Sci Heat Treat* 59: 297–301. https://doi.org/10.1007/s11041-017-0146-5
8. Chyła P, Pater Z, Tomczak J, et al. (2016) Numerical analysis of a rolling process for producing steel balls using helical rolls. *Arch Metall Mater* 61: 485–492. https://doi.org/10.1515/amm-2016-0085

9. Hao Y, Li J, Li X, et al. (2020) Influences of cooling rates on solidification and segregation characteristics of Fe-Cr-Ni-Mo-N super austenitic stainless steel. *J Mater Process Technol* 275: 116236. https://doi.org/10.1016/j.jmatprotec.2019.116326
10. Zai L, You G, Tong X, et al. (2020) Microstructure and mechanical properties of inertia-friction-welded Fe-Cr-Ni-Mo high-strength steel. *Steel Res Int* 91: 1–12. https://doi.org/10.1002/srin.202000145
11. Sabih A, Radziszewski P, Mullany I (2017) Investigating grinding media differences in microstructure, hardness, abrasion and fracture toughness. *Miner Eng* 103: 43–53. https://doi.org/10.1016/j.mineng.2016.08.014
12. Efremenko VG, Popov ES, Kuz'Min SO, et al. (2014) Introduction of three-stage thermal hardening technology for large diameter grinding balls. Metallurgist 57: 849–854. https://doi.org/10.1007/s11015-014-9812-7
13. Çolak SS, Altun O, Benzer H, et al. (2018) Development of a preliminary media wear measurement test procedure for cement ball milling applications. *Powder Technol* 325: 678–686. https://doi.org/10.1016/j.powtec.2017.11.033
14. Daraio D, Villoria J, Ingram A, et al. (2020) Investigating grinding media dynamics inside a vertical stirred mill using the discrete element method: Effect of impeller arm length. *Powder Technol* 364: 1049–1061. https://doi.org/10.1016/j.powtec.2019.09.038
15. Jang JW, Iwasaki I, Moore JJ (1989) Effect of galvanic interaction between martensite and ferrite grinding media wear. *Corrosion* 45: 402–407. https://doi.org/10.5006/1.3582036
16. Jurči P, Dománková M, Čaplovič Ľ, et al. (2015) Microstructure and hardness of sub-zero treated and no tempered P/M Vanadis 6 ledeburitic tool steel. *Vacuum* 111: 92–101. https://doi.org/10.1016/j.vacuum.2014.10.004
17. Murthy BRN, Rangappa R (2021) Morphology and wear of high chromium and austempered ductile iron balls as grinding media in ball mills. *J Phys-Conf Ser* 2070: 012201. https://doi.org/10.1088/1742-6596/2070/1/012201
18. Das D, Ray KK (2012) Structure-property correlation of sub-zero treated AISI D2 steel. *Mater Sci Eng A-Struct* 541: 45-60. https://doi.org/10.1016/j.msea.2012.01.130
19. Sobotova J, Ku-Gik M, Krum S, et al. (2016) Effect of sub-zero treatment on the wear resistance of P/M tool steels. *J Appl Mech Eng* 5: 1000243.
20. Jurči P, Bartkowska A, Hudáková M, et al. (2021) Effect of sub-zero treatments and tempering on corrosion behaviour of vanadis 6 tool steel. *Materials* 14: 3759. https://doi.org/10.3390/ma14133759
21. Kosaraju S, Singh SK, Buddi T, et al. (2020) Evaluation and characterisation of ASS316L at sub-zero temperature. *Adv Mater Process Technol* 6: 445–455. https://doi.org/10.1080/2374068X.2020.1728650
22. Shah N, Arora K, Dhokey NB, et al. (2019) Studies on wear behaviour and DBTT in sub-zero regimes of cryo-treated high nitrogen martensitic stainless steel (HNMS). *Trans Indian Inst Met* 72: 2121-2126. https://doi.org/10.1007/s12666-018-01555-2
23. Zhou Q, Luo D, Hua D, et al. (2022) Design and characterization of metallic glass/graphene multilayer with excellent nanowear properties. *Friction* 10: 1913–1926. https://doi.org/10.1007/s40544-021-0581-6

24. Yan XG, Li DY (2013) Effects of the sub-zero treatment condition on microstructure, mechanical behavior and wear resistance of W9Mo3Cr4V high speed steel. *Wear* 302: 854–862. https://doi.org/10.1016/j.wear.2012.12.037
25. Li DH, He WC, Zhang X, et al. (2021) Effects of traditional heat treatment and a novel deep cryogenic treatment on microstructure and mechanical properties of low-carbon high-alloy martensitic bearing steel. *J Iron Steel Res Int* 28: 370–382. https://doi.org/10.1007/s42243-020-00527-5
26. Szala M, Winiarski G, Wójcik Ł, et al. (2020) Effect of annealing time and temperature parameters on the microstructure, hardness, and strain-hardening coefficients of 42CrMo4 Steel. *Materials* 13: 1–16. https://doi.org/10.3390/ma13092022
27. Zhirafar S, Rezaeian A, Pugh M (2007) Effect of cryogenic treatment on the mechanical properties of 4340 steel. *J Mater Process Technol* 186: 298–303. https://doi.org/10.1016/j.jmatprotec.2006.12.046
28. Shamsolhodaei A, Oliveira JP, Schell N, et al. (2020) Controlling intermetallic compounds formation during laser welding of NiTi to 316L stainless steel. *Intermetallics* 116: 106656. https://doi.org/10.1016/j.intermet.2019.106656
29. Wang K, Gu K, Miao J, et al. (2019) Toughening optimization on a low carbon steel by a novel Quenching-Partitioning-Cryogenic-Tempering treatment. *Mater Sci Eng A-Struct* 743: 259–264. https://doi.org/10.1016/j.msea.2018.04.104
30. Akincioğlu S, Gökkaya H, Uygur I (2015) A review of cryogenic treatment on cutting tools. *Int J Adv Manuf Technol* 78: 1609–1627. https://doi.org/10.1007/s00170-014-6755-x
31. Gill SS, Singh J, Singh R, et al. (2012) Effect of cryogenic treatment on AISI M2 high speed steel: Metallurgical and mechanical characterization. *J Mater Eng Perform* 21: 1320–1326. https://doi.org/10.1007/s11665-011-0032-z
32. Wang LY, Wu YX, Sun WW, et al. (2020) Strain hardening behaviour of as-quenched and tempered martensite. *Acta Mater* 199: 613–632. https://doi.org/10.1016/j.actamat.2020.08.067
33. Patil PI, Tated RG (2012) Comparison of effects of cryogenic Treatment on different types of steels: A review. *International Conference in Computional Intelligence (ICCIA)* 9: 10–29.
34. Jovičević-Klug P, Jovičević-Klug M, Sever T, et al. (2021) Impact of steel type, composition and heat treatment parameters on effectiveness of deep cryogenic treatment. *J Mater Res Technol* 14: 1007-1020. https://doi.org/10.1016/j.jmrt.2021.07.022
35. Alqarni ND, Wysocka J, El-Bagoury N, et al. (2018) Effect of cobalt addition on the corrosion behavior of near equiatomic NiTi shape memory alloy in normal saline solution: Electrochemical and XPS studies. *RSC Adv* 8: 19289–19300. https://doi.org/10.1039/C8RA02031K
36. Wang XH, Zhong SY, Song YH, et al. (2020) Effect of tantalum film on corrosion behaviour of AA6061 aluminium alloy in hydrochloric acid- and chloride-containing solutions. *Trans Inst Met Finish* 98: 243–249. https://doi.org/10.1080/00202967.2020.1802930
37. Zhou X, Liao C, Wang Y, et al. (2021) Constructing the Pourbaix diagram of Fe-Cl^--H_2O ternary system under supercritical water conditions. Electrochim Acta 377: 138075. https://doi.org/10.1016/j.electacta.2021.138075
38. Utomo EP, Herbirowo S, Puspasari V, et al. (2021) Characteristics and corrosion behavior of Ti-30Nb-5Sn alloys in histidine solution with various NaCl concentrations. *Int J Corros Scale Inhib* 10: 592–601. https://doi.org/10.17675/2305-6894-2021-10-2-7

39. Hu J, Zhu Y, Hang J, et al. (2021) The effect of organic core-shell corrosion inhibitors on corrosion performance of the reinforcement in simulated concrete pore solution. *Constr Build Mater* 267: 121011. https://doi.org/10.1016/j.conbuildmat.2020.121011
40. Li S, Xiao M, Ye G, et al. (2018) Effects of deep cryogenic treatment on microstructural evolution and alloy phases precipitation of a new low carbon martensitic stainless bearing steel during aging. *Mater Sci Eng A-Struct* 732: 167–177. https://doi.org/10.1016/j.msea.2018.07.012
41. Samuel AP, Arul S (2018) Effect of cryogenic treatment on the mechanical properties of low carbon steel IS 2062. *Mater Today Proc* 5: 25065–25074. https://doi.org/10.1016/j.matpr.2018.10.307
42. Liao J, Li L, Peng J, et al. (2020) Effects of deep cryogenic treatment on the microstructure and friction performance of M35 high-speed steel. *J Phys-Conf Ser* 1676: 012098. https://doi.org/10.1088/1742-6596/1676/1/012098
43. Sendya A, Marzuki H, Herbirowo S, et al. (2020) Study of Cr/Mo alloys lateritic steel with the soaking time cryogenic treatment on hardness, toughness, abrasive resistant, and microstructure. *Met Indones* 42: 21–27. https://doi.org/10.32423/jmi.2020.v42.20-27
44. Jia Q, He W, Hua D, et al. (2022) Effects of structure relaxation and surface oxidation on nanoscopic wear behaviors of metallic glass. *Acta Mater* 232: 117934. https://doi.org/10.1016/j.actamat.2022.117934

AIMS Press

© 2023 the Author(s), licensee AIMS Press. This is an open access article distributed under the terms of the Creative Commons Attribution License (http://creativecommons.org/licenses/by/4.0).